LANGMUIR

pubs.acs.org/Langmuir Article

Surfactant-Mediated Solubilization of Myelin Figures: A Multistep Morphological Cascade

Daniel J. Speer, James C. S. Ho, and Atul N. Parikh*

Cite This: *Langmuir* 2022, 38, 8805−8816 Read Online

ACCESS | Metrics & More | Article Recommendations | Supporting Information

ABSTRACT: Lamellar mesophases of insoluble lipids are readily solubilized by the micellar mesophases of soluble surfactants. This simple process underscores a broad array of biochemical methodologies, including purification, reconstitution, and crystallization of membrane proteins, as well as the isolation of detergent-resistant membrane fractions. Although much is now known about the thermodynamic driving forces of membrane solubilization, the kinetic pathways by which the surfactant alters vesicular mesophases are only beginning to be appreciated. Little is known about how these interactions affect the solubilization of more complex, multilamellar mesophases. Here, we investigate how a common zwitterionic detergent affects the solubilization of a smectic, multilamellar, cylindrical mesophase of lipids, called the myelin figure. Our results reveal that myelin solubilization occurs in a multistep manner, producing a well-defined sequence of morphologically distinct intermediates *en route* to complete solubilization. The kinetic processes producing these intermediates include (1) coiling, which encompasses the formation, propagation, and tightening of extended helices; (2) thinning, which reflects the unbinding of lamellae in the smectic stacks; and (3) detachment or retraction, which either dissociates the myelinic protrusion from the source lipid mass or returns the myelinic protrusion to the source lipid mass—all in transit toward complete solubilization. These occasionally overlapping steps are most pronounced in single-lipid component myelins, while compositionally graded multicomponent myelins inhibit the coiling step and detach more frequently. Taken together, the appearance of these intermediates during the solubilization of myelins suggests a complex free-energy landscape characterizing myelin solubilization populated by metastable, morphological intermediates correlated with locally minimized changes in energy dependent upon the mesophase's composition. This then predicts the accessibility of structurally distinct, kinetic intermediates—such as loose and tight coiled helices, peeled myelins, retracted tubes, and detached protrusions—before reaching the stable ground state corresponding to a dissolved suspension of mixed surfactant−lipid micelles.

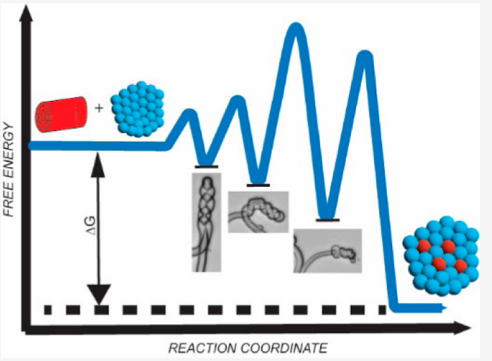

INTRODUCTION

Molecular components of biological membranes—phospholipids, glycolipids, sterols, and membrane proteins—are insoluble amphiphiles.[1,2] Taken alone, they spontaneously aggregate in aqueous media, forming smectic liquid-crystalline, lamellar mesophases, or insoluble precipitates.[3,4] Surfactants and detergents, by contrast, are soluble amphiphiles.[1] Above a threshold concentration—the critical micelle concentration (CMC)—they form micelles in water.[2,4] When these two hydrophobically assembled mesophases—one comprising insoluble lipids and the other soluble surfactants—interact, complex dynamics ensue.[5] In a typical case, the surfactant from the micellar phase invades the lipidic mesophase, thereby driving it far outside the thermal equilibrium.[6−8] The subsequent evolution of this nonequilibrium state, as it progresses toward a new equilibrium, is often complicated: it is dominated by the rates and manners by which the surfactant dopes in the parent mesophase and how it perturbs, evolves, and modifies the initial morphology.[9−13]

This is perhaps best exemplified by the common biochemical process of detergent-mediated membrane solubilization.[6,8] Detergents (or surfactants), used extensively to extract, purify, and reconstitute membrane proteins and isolate detergent-resistant lipid rafts, destabilize the bilayer motif, ultimately leading to complete solubilization of the target membrane.[14−20] A sequence of complex and reversible phase transformations accompany membrane solubilization, the qualitative phenomenology of which is captured elegantly by the so-called three-stage model. First proposed by Helenius and Simons in 1975, the consensus model distinguishes three stages of equilibration or morphological evolution.[8] Stage 1 represents a state characterized by an effective concentration of detergents in a membrane (or detergent-lipid ratio, R_e) below a threshold saturation value ($R_e < R_e^{sat}$). Here, detergent binds

Received: March 25, 2022
Revised: June 24, 2022
Published: July 11, 2022

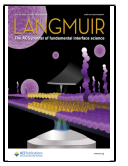

https://doi.org/10.1021/acs.langmuir.2c00774
Langmuir 2022, 38, 8805−8816

and partitions into the bilayer. The resulting diversification of mass, area, composition, tension, and curvature alters the physical properties of the membrane. In stage 2, when the membrane is saturated with the detergent ($R_e^{sat} < R_e < R_e^{sol}$), a characteristic lamellar-to-micellar phase transition produces large, lipid-saturated mixed micelles that coexist in equilibrium with the residual lamellar bilayer. Beyond solubilizing detergent concentrations ($R_e \geq R_e^{sol}$), which represents stage 3, the lamellar phase is fully solubilized. Here, the entropic mixing between large, lipid-detergent mixed micelles and small, pure detergent micelles stabilizes smaller detergent-saturated mixed micelles at equilibrium. These three stages, which describe shifting equilibria corresponding to increasing surfactant concentrations, are thought to map onto the temporal steps characterizing the morphological evolution that ensues when membranes encounter detergents at solubilizing concentrations (>CMC).[6,21]

Conspicuously absent in this picture—which treats different aggregates (and monomers) as distinct thermodynamic pseudophases in equilibrium with one another—are the dynamics and specificities of interactions between the surfactant and the lipidic mesophase.[9,22] This is perhaps best illustrated by a recent study examining the dynamics of interactions between surfactants and giant unilamellar vesicles (GUVs) in real time.[9] The investigation documents a striking diversity of kinetic pathways that characterize the membranous dissolution dynamics. Some of the characteristic pathways that the study identifies involve continuous shrinking, inside-out topological inversions, site-directed openings, and rapid bursting of GUVs. Each of these pathways is a consequence of how surfactants intercalate into and organize within the membrane; none are predicted by the equilibrium three-stage model.[9] Other more recent investigations confirm these findings and further reveal a plethora of additional, qualitatively different phase and morphological transformations that accompany membrane solubilization when lipid compositions are altered, and other classes of amphiphilic surfactants are used.[23−27]

These nuances of the surfactant−mesophase interactions, namely, the specificities of how surfactants partition within the membrane and the types of deformations they elicit, become exacerbated when the solubilizing morphology is a structurally complex mesophase. Consider, for example, a multilamellar, smectic phase of lipids. In these hierarchically organized mesophases, only the outermost lamellae are initially available for interaction with added surfactants. Thus, the solubilization must proceed in a multistep cascade with each subsequent lamellae interacting with the micelles of the surfactant and mixed micelles of varying compositions produced by its interactions with preceding lamellae. Furthermore, morphological changes, which follow when the surfactant enters the lamellar mesophases, are constrained by the interlamellar interactions (i.e., Helfrich interactions) holding the smectic layers together.[28] Finally, any compositional differences, such as those that may exist in the layers of the parent mesophase, must also alter the kinetics and thermodynamics of solubilization. How these structural complexities influence the abilities of surfactants to solubilize complex mesophases is largely unknown.

Motivated by these considerations, we investigate here the surfactant-induced solubilization of a novel class of lyotropic, cylindrical, smectic mesophase called the myelin figure. First reported by Virchow more than 150 years ago, these mesophases appear as a dense tangle of tubules when water encounters a dried mass of nearly insoluble ($\sim 10^{-10}$ M) lipids.[29−33] These finger-like protrusions—which are tens of micrometers wide and extend to hundreds of micrometers in length—nest thousands of cylindrically stacked, alternating lamellae of lipid bilayers and aqueous channels wrapping a narrow (~100 nm), central, aqueous core.[30,34,35] Their 1D smectic order is stabilized by the interlamellar Helfrich repulsion, which separates the neighboring bilayers by nanometer-scale aqueous channels and inhibits molecular exchanges between individual lamellae.[28] Previous research efforts have explored the perturbations of the myelinic organization with amphiphilic, aqueous-soluble dopants, finding that the tubes morphologically transition from linear tubes to coiled helices.[36] While valuable for our understanding of myelin behavior, these molecular dopants did not undertake any solubilizing action.

In our study, the solubilizing detergent of choice was the synthetic zwitterionic surfactant Zwittergent 3−12 (*n*-dodecyl-*N*,*N*-dimethyl-3-ammonio-1-propanesulfonate or DDAPS, CMC = 2−4 mM), which is used widely in the isolation of membrane proteins.[37−40] Both single-lipid component and multicomponent myelins were studied. Single-component myelins were prepared using fluid-phase 1-palmitoyl-2-oleoyl-*sn*-glycero-3-phosphocholine (POPC), and multicomponent myelins comprised an equimolar mixture of POPC, cholesterol (CHOL), and egg sphingomyelin (SM). In both cases, either the dried lipid mass was hydrated using the detergent-laden aqueous solution or the preformed myelins were exposed to solutions of DDAPS. The resulting myelinization and morphological changes were monitored in real time using brightfield, confocal fluorescence, and wide-field fluorescence microscopies.

The results reported here establish that the DDAPS-mediated dissolution of myelins is neither direct nor independent of myelin molecular composition. *En route* to complete solubilization, the chemically homogeneous single-component myelins composed of fluid-phase POPC lipids undergo a sequence of well-defined morphological changes before undergoing complete solubilization. These steps include coiling, which encompasses the formation, propagation, and tightening of extended helices, thinning, reflecting the unbinding of smectic lamellae, and retraction. In sharp contrast, the dissolution of multicomponent myelins consisting of phase-separating ternary mixtures of POPC, CHOL, and SM—which are known to form compositionally graded myelins—exhibit little or no propensity for coiling but undergo gradual thinning, as well as retraction or detachment.[41] The appearance of these intermediates during the dissolution of myelins suggests a complex free-energy landscape of myelin solubilization, possibly parallel to the one predicted by Ostwald's rule of stages.[42]

RESULTS AND DISCUSSION

Preliminary characterization of the hydration of the single-component mother lipid reservoir (or "lipid cake") by pure water was carried out to confirm myelinization. Upon contacting water, the boundaries of dried POPC cakes roughen instantaneously. A dense tangle of well-defined myelin figures projecting into the aqueous phase decorates the lipid−water interface, confirming the essential phenomenology.

Although individual myelins meander and grow sinuously, the average length—the distance (l) between the front

https://doi.org/10.1021/acs.langmuir.2c00774
Langmuir 2022, 38, 8805−8816

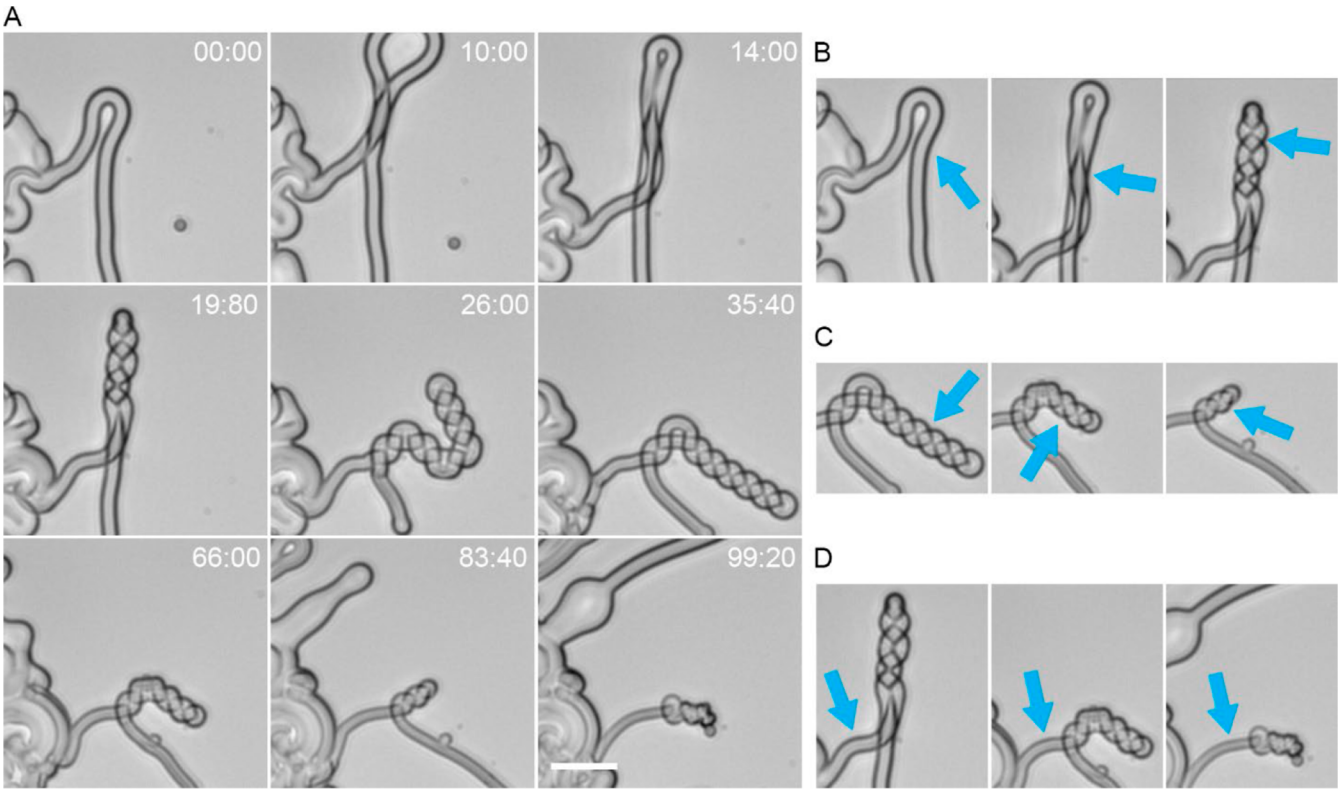

Figure 1. Detergent-mediated shape remodeling of single-component myelin figures. (A) Selection of time-lapse brightfield microscopy images of a representative myelin figure consisting of 100 mol % POPC lipids coiling and dissolving in an aqueous solution containing 120 mM DDAPS. The example reveals a single, flexible myelin looping, twisting, and coiling to form an extended helix propagating away from the tip of the loop. With time, the myelin thins, uncoils, and retracts back to the mother lipid mass. Time stamp, sec:centisec; scale bar, 20 μm. (B–D): Cropped images highlight the overlapping development of the (B) loose coiled state, (C) tight coiled state, and (D) peeled state marked by arrows.

extending into the water and the root at the base of the lipid cake—for a collection of myelins in single experiments showed a characteristic growth pattern: on average, myelins grew with a square root of time ($l \propto t^{1/2}$) dependence (Figure S1). This growth pattern is fully consistent with previous observations and lends further credence to the preponderance of diffusive mechanisms in determining myelinic growth: a combination of (1) collective diffusion of lipid aggregates in response to the hydration gradient at the lipid–water interface and (2) lateral diffusion of lipids within the bilayer.[31,43−45] Quantifying the growth ($l^2 = k\,t + c$), we find that the apparent diffusion constant, k, is $3.00 \times 10^{-6} \pm 0.02$ cm^2/s ($n = 3$) during the first 60 s of growth, which is comparable to the range of values reported previously (4.3×10^{-6} cm^2/s for a hen-egg lipid mixture, 2.0×10^{-6} cm^2/s for an unspecified phosphatidylcholine lipid, 7.0×10^{-7} cm^2/s for the amphiphile $C_{12}E_3$, 2.2×10^{-6} cm^2/s for the amphiphile $C_{12}E_6$, and 1.0×10^{-6} cm^2/s for egg-PC at room temperature).[43,44,46−48] Although infrequent, we occasionally observed that the linearly protruding myelins coiled spontaneously, typically within the first few minutes (2–3 min) of hydration (Video S1). Examining the behaviors of a large number of myelins ($n = 253$), we find that this spontaneous higher-order organization is both stochastic and rare, measuring at 0.4% of all myelins examined.

Substituting the hydrating solution with one containing DDAPS at concentrations above its CMC (2–4 mM), we find a dramatic shift. Although the lipid–water interface roughened and tubular myelins projected into the aqueous phase at comparable growth rates as above, the protrusions abandoned their linear morphologies. Instead, a statistically significant proportion of myelins, far surpassing the 0.4% above (see below), exhibited extended coiling—a higher-order organization breaking the chiral symmetry of the stacked myelin membranes. In sharp contrast, the giant vesicle, an exemplary, single-component, unilamellar mesophase, did not express such unique morphological developments in its solubilization (Videos S2, S3, S4, S5, and S6). The vesicular organization catastrophically ruptured when exposed to comparable concentrations of DDAPS.

Real-time visualization of this gross shape remodeling (Figure 1) reveals a rapid propagation of an initial stochastically generated, localized twist along the length of the myelin, often producing extended helices spanning the length of myelin figures themselves (>50 μm). The twisting motif forming the helices was also substantially diverse: both self-coiling (single strands) and, less commonly, cross-coiling of neighboring myelins producing double helices were evident, often in single samples (Video S7). The former, self-coiling, is propagated by the generation of new pitches from a twisting deformation of a hairpin loop connecting the two arms, and the latter, cross-coiling, occurs through the helical coiling of separate myelins around one another. Moreover, there appeared to be little or no discernible preference for the sense of winding direction (handedness): roughly, 45% were left-handed, 42% were right-handed, and 13% had both left- and right-handed sections on a single pair of strands ($n = 60$).

By performing myelinization experiments using aqueous solutions with systematically varied DDAPS concentrations (1, 5, 15, 30, 60, 90, and 120 mM), we found that the surfactant

https://doi.org/10.1021/acs.langmuir.2c00774
Langmuir 2022, 38, 8805−8816

concentration had a profound effect on the prevalence of this higher-order organization (Figure 2). At low surfactant

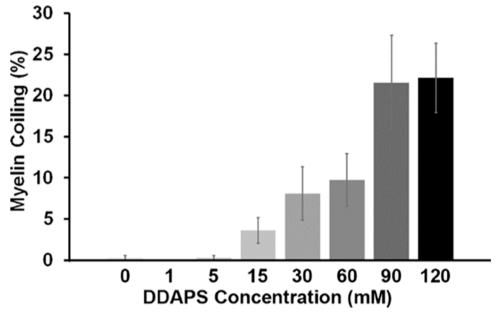

Figure 2. Detergent concentration-dependent coiling of myelin figures. With increasing DDAPS concentration (0−120 mM) in the hydrating solution, the proportion of individual POPC myelins undergoing a coiling transition within the first 5 min of hydration increases monotonically. The error bars represent the standard error of means (n = 5).

concentrations—in the vicinity of the CMC value of DDAPS (2−4 mM)—the myelins formed were essentially indistinguishable from those produced in pure water. In other words, they were largely unperturbed by the presence of the surfactant and displayed a clear tendency to form linear myelins extending several times their diameters. At and above 15 mM surfactant concentration, however, noticeably higher fractions of myelins displayed the appearance of the coiling motif. Quantifying the myelin landscape, we find that the number fractions of coiled myelins grew with the surfactant concentration: 3.57 ± 1.55% (n = 5) at 15 mM to 22.14 ± 4.20% (n = 5) at 120 mM (Figure 2).

The formation of a coil necessitates the consolidation of the length of the tube, effectively reducing the extension of the myelinic protrusion. This could be achieved by shortening the linearly extending tube or consolidating additional growth. Our observations provide evidence for each of the two mechanisms. Our results reveal that the surfactant-induced coiling can recruit existing portions of the essentially linear sections of a myelin (Videos S8 and S9), iron out any available wrinkles of sinuous sections of a myelin (Figure S2), or access additional tube length made available by the growth of a myelin (Video S10). Over time, helical myelins exhibited a consistent pattern of tightening (Videos S11, S12, and S13). While the diameters of uncoiled segments of participating myelins remained unchanged, the helices contracted: the pitch length—the length of a complete helical turn, measured along the helical axis—decreased, and the width—the largest size perpendicular to the central axis—shrank (Figure 3). This gradual tightening of the helical coil, which increases the contact surface at the cost of bending the tube, is consistent with the notion that surface adhesion plays a role.[49] Notably, as the helices tightened, the pitch angle—defined as the arc tangent of the ratio of the tube diameter to the pitch length—remained essentially unchanged, hovering around an average of ∼39° (Figure S3). This then suggests that the two processes, the tightening of the helical segments and the thinning of the tubes, occur concurrently.

Visualizing the fate of the coiled myelins over the long term, we find that the coiled state is not permanent. Overtime ($t \geq 5$ min), helical myelins solubilized into the surrounding bath. This unraveling is gradual: the coiled myelins become thin, uncoil, retract, and dissolve (Figure S2). The observation of solubilization is confirmed by monitoring the base of a helix: linear myelin tubes at the root of the helix thinned or peeled as their external bilayers underwent delamination reminiscent of a lamellar unbinding transition (Figures 3 and S2D).[50]

Real-time visual analysis of the base of the helices reveals a rate independent of the surfactant concentration (Figure 3E). Moreover, we find that the average solubilization kinetics yields a rate constant of $k \sim 0.01$ μm/s for the solubilization process. Assuming the myelin tube to be a smooth cylinder and using the approximations of each bilayer's thickness to be 5 nm

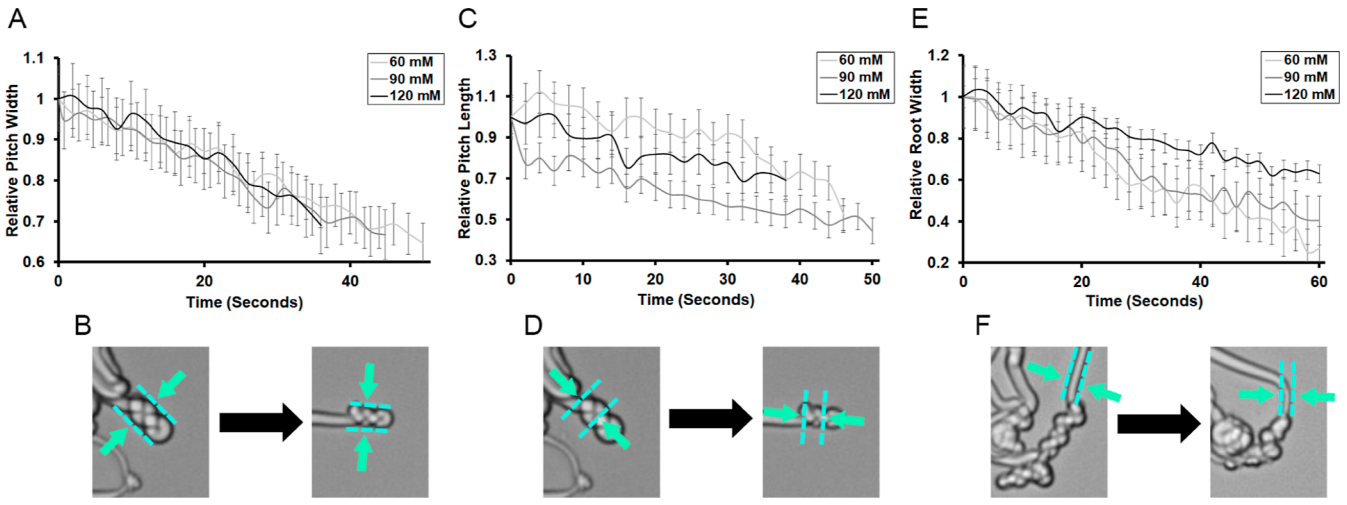

Figure 3. Coil tightening and myelin thinning stages during DDAPS-mediated solubilization of single-component myelin figures. (A) The relative width (in comparison to the starting observed width) of the helical morphology was measured in real time at various concentrations of DDAPS. Error bars, standard error based on image resolution, ±0.4 μm. (B) The helical width of myelin was measured as depicted by the distance between the dashed lines of the selected images. (C) The relative length of the helical pitches was measured vs time in a similar comparative manner to (A). (D) The helical pitch length of myelin was measured as depicted by the distance between the dashed lines of the selected images. (E) The relative width of the roots of the helical morphologies was measured over time to investigate the dissolution rate of the available bilayers. (F) The helical root width of myelin was measured as depicted by the distance between the dashed lines of the selected images.

https://doi.org/10.1021/acs.langmuir.2c00774
Langmuir 2022, 38, 8805−8816

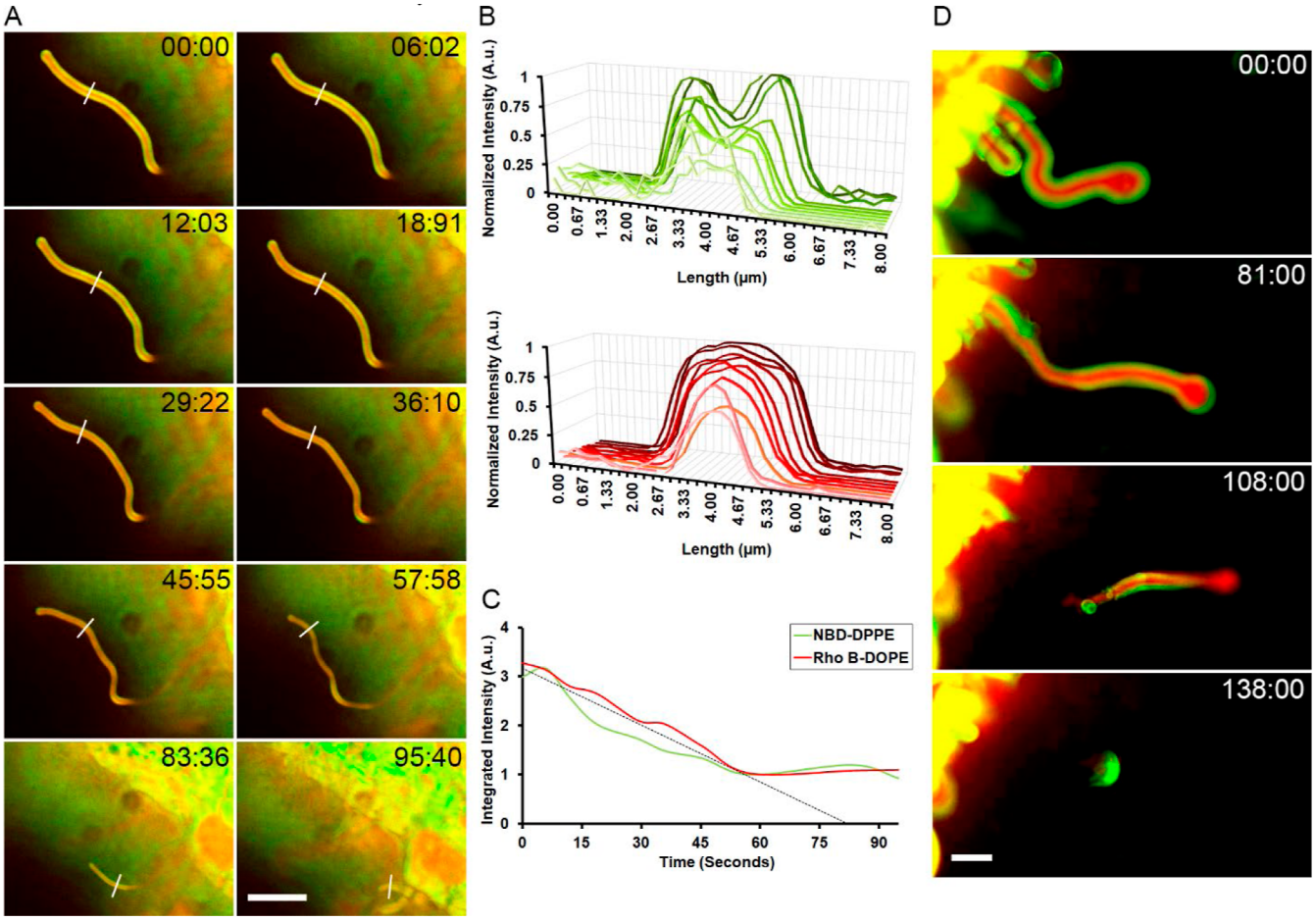

Figure 4. Solubilization and detachment of compositionally graded multicomponent myelins. (A) Time-lapse depiction of a multicomponent myelin composed of a 1:1:1 ratio of POPC, SM, and CHOL with 0.1 and 0.3 mol % Rho B-DOPE and NBD-DPPE dopants (respectively) showing thinning and retraction. The white line on each frame depicts the line along which fluorescence intensity was measured for (B). Time stamp, sec:centisec; scale bar, 20 μm. (B) The fluorescence intensities of both the NBD-DPPE (green) and Rho B-DOPE (red) channels of the multicomponent myelin figure were measured along the length of the manually drawn normal line and normalized to their average background intensity. Normalized fluorescence plots for both channels were measured throughout time and plotted together where the time points are 0 s (darkest shade), 6.02 s, 12.03 s, 18.91 s, 29.22 s, 36.10 s, 45.55 s, 57.58 s, 83.36 s, and 95.40 s (lightest shade). (C) The normalized intensity was integrated to elucidate the area under the curve at each time point for each channel. Integrated intensity data was plotted vs time for each channel. A trendline of the initial thinning is also plotted with a slope of k ~ 0.04. (D) Time-lapse depiction of a multicomponent myelin composed of a 1:1:1 ratio of POPC, SM, and CHOL with 0.1 mol % and 0.3 mol % Rho B-DOPE and NBD-DPPE dopants (respectively) detaching from the lipid cake and solubilizing as a free-floating myelin. Time stamp, sec:centisec; scale bar, 20 μm.

and each phospholipid's lateral area to be 0.65 nm^2, we can calculate an approximate rate of material loss from the myelin figures.[51] Using this estimated rate constant, a singular myelin tube is losing roughly two bilayers per unit length per second or ~9.75 × 10^{-18} mol POPC/(sec) (μm length) or ~5.87 × 10^7 POPC molecules/(sec) (μm length) because of its interactions with DDAPS in solution (Figure S4 and Videos S8, S9, and S14). These intermediate stages did not always appear as well-separated sequential events. In several instances, at the time resolution of 0.2 s per frame in our measurements, certain states seemed to be skipped, whereas others appeared to proceed concurrently (Figures S2 and S4).

A unique feature of the multilamellar myelinic organization is that it can stabilize gradients in chemical composition between lamellae.[41] In multicomponent lipid mixtures, where different lipids hydrate and fluidize differently, the myelinic organization preserves the record of differences in their hydration kinetics. In a recent study, we have shown that this can give rise to long-lived spatial patterns of chemical composition. Specifically, we found that when lipid cakes containing phase-separating mixtures of unsaturated lipid, cholesterol, and sphingomyelin are hydrated, interlamellar molecular segregation ensues. The resulting myelins display continuous, interlamellar radial gradients of concentrations of cholesterol, sphingomyelin, and the unsaturated lipid. The latter fluid-phase lipids concentrate in the inner lamellae and the former lipids, cholesterol and sphingomyelin, accumulate in the outer lamellae at the highest concentrations. An immediate consequence of this compositional gradient is that the outermost, cholesterol-enriched lamellae are stiffer and more resistant to solubilization by detergent.[6,21,52,53] How would such graded organizations influence the abilities of surfactants to drive solubilization? Would it help shield the buried fluid-phase lamellae within a protective coat of cholesterol-rich outer layers?

Myelin figures were assembled using a 1:1:1 molar ratio of POPC, SM, and CHOL with 0.1 mol % Rho B-DOPE and 0.3 mol % NBD-DPPE dopants (respectively) as fluorescent dyes,

https://doi.org/10.1021/acs.langmuir.2c00774
Langmuir 2022, 38, 8805−8816

which labeled the liquid-disordered (L_d) and liquid-ordered (L_o) phases, respectively. Upon hydration with an aqueous solution, the L_o phase preferentially partitioned to the external bilayers and the L_d phase preferred the internal core of the myelin figures, confirming previous work.[41]

Hydration with aqueous solutions containing DDAPS (90 mM) triggered the solubilization of these multicomponent myelins. During the ∼10 min following hydration, multicomponent myelins displayed continuous thinning (Videos S15 and S16). Of the many instances of myelin dynamics observed (n = 518), none coiled, and no helices were observed over tens of minutes of observation. Quantifying the thinning dynamics by monitoring the changes in the fluorescence of the two phase-sensitive lipid probes, Rho B-DOPE and NBD-DPPE, yielded further insights (Figure 4). When integrated and averaged, both channels displayed a thinning rate of $k \sim 0.04$, 4 times higher than that during the solubilization of the single-component POPC myelins. Using the same approximations as above, the myelin tube sheds roughly eight bilayers per unit length per second or $\sim 2.39 \times 10^{-16}$ mol POPC/(sec) (μm length) or $\sim 1.44 \times 10^{8}$ POPC molecules/(sec) (μm length) during the thinning stage. Monitoring the changes in the integrated fluorescence due to the two phase-sensitive dyes, we observe that the two—the NBD-DPPE channel pertaining to the external L_o phase and the Rho B-DOPE channel pertaining to the internal L_d—decay at comparable rates. This difference can be straightforwardly understood by considering the phase dependence of surfactant partitioning and accessibility. Although the L_d phase is less abundant in the exposed leaflets, the greater partitioning of DDAPS within that phase might account for increased local destabilization, thereby yielding comparable apparent rates of delamination of the L_d and L_o phase components during thinning (Figure 4C).

The DDAPS-mediated thinning of multicomponent myelins was accompanied by another notable difference. A subpopulation of thinning myelin figures shortened in length, ultimately retracting to the mother lipid mass. An equally significant proportion of myelins displayed a remarkable topological transition, detaching the myelinic protrusions from the mother lipid mass and producing freely suspended tubules (Figure 4D and Video S17). These isolated, discrete myelins are not long-lived: over time, their tubular geometry is abandoned, producing rounded mesophases *en route* to dissolving entirely. This general trend in surfactant-mediated morphological transitions was fully reproducible for different compositions of the ternary myelins. Changing the 1:1:1 lipid ratio to a 3:1:1 and 1:2:2 ratio of POPC, SM, and CHOL revealed qualitatively comparable solubilization dynamics (Videos S18 and S19).

Given the differentiated morphogenesis observed above, several factors must be considered to appreciate the kinetic and thermodynamic determinants of these unusual solubilization trajectories. First, is the coiling of myelin tubes. Previous research efforts have deduced a number of mechanistic explanations for coiling depending on their observational contexts. First, helical coils of myelin tubes were hypothesized to originate from an adhesion force between the surface bilayers. This could manifest as either an electrostatic interaction between involved, negatively charged head-group lipids and dissolved cations or intermembrane interactions between neutrally charged lipids.[49,54,55] Using some empirical estimates, the attractive force outcompeted the energetic cost of bending bilayers in the tube. A confounding study showed that adhesion does not solely induce coiling; moreover, the presence of external, amphiphilic dopants could. Using the biopolymer dextran grafted with 16 carbon aliphatic chains, myelin tubes began to coil more frequently.[36,56] Here, the polymer becomes an integral part of the myelin composition, doping each lamella of the multilamellar myelin architecture. These studies propose that the coiling of myelins arises because of the local polymer concentration, which induces spontaneous curvature, and the mobility of the polymer along the length of the myelin, which reduces the bending energy penalty. Lastly, an independent theoretical study identifies that a coiling instability may also emerge when nonexternally perturbed myelin's lamellae are compressed, such as under osmotic stress, which acts to reduce the equilibrium distance between the lamellar membranes.[57] In these cases, the curvature energy penalty, which resists the decrease in radii of membrane lamellae, competes with the relaxation to the new equilibrium. This then sets the stage for a buckling instability—akin to a Helfrich−Hurault instability—promoting coiling.[58,59] In the present case, the relevant, confounding hypotheses can be assimilated for a holistic understanding of myelin behavior. We begin by eliciting the interactions between the doped surfactant and the myelinic lamellae. They are determined by the kinetics and thermodynamics of (1) how DDPAS spatially distributes within the bilayer, distributing homogeneously or accumulating locally in mesophase domains; (2) how it partitions between the two leaflets of each bilayer; and (3) how the intercalation of the surfactant influences the flip-flop translocation of lipids comprising the myelin, ultimately producing mixed micelles. Previous studies establish that the intercalation of DDAPS in the exposed, outermost bilayer is rapid. The partitioning coefficients of DDAPS, K_p (mol l^{-1} in the membrane/mol l^{-1} in the aqueous phase), have been reported to range from thousands to tens of thousands.[60] However, the subsequent distribution of DDAPS between the leaflets of the exposed bilayer is considerably limited, presumably because of DDAPS's zwitterionic head-group and positive molecular curvature.[60] Together, these behaviors promote the localized accumulation of DDAPS in outer leaflets of the exposed bilayer, asymmetrically expanding the bilayer, producing detergent-enriched domains, and generating curvature stress.[6] To relieve this elastic stress, single bilayers bend to assume the corresponding local spontaneous curvature, as predicted by the so-called bilayer-couple hypothesis.[61] The bending of single leaflets, however, is strongly opposed by the interleaflet interactions and the interlamellar Helfrich interactions.[28] A slow morphological consequence of this tug-of-war between competing influences of local spontaneous curvature and interlamellar interactions—deduced previously in theoretical formulations based on equilibrium considerations—is the breaking of the stack's chiral symmetry, leading to coiling.[36,56,57] These competing forces, as well as other factors such as the mass transfer of both pure DDAPS micelles to and mixed micelles from the parent mesophase, dictate the kinetics of this process and explain why the solubilization rate appears to be independent of concentration.[62]

In contrast, how is the coiling step suppressed when utilizing compositionally graded, multicomponent myelins? Our results robustly demonstrate that the myelins produced by the mixtures of POPC, cholesterol, and sphingomyelin exhibit little or no propensity for coiling. As shown previously, and confirmed here, individual lamellae of myelins produced by

https://doi.org/10.1021/acs.langmuir.2c00774
Langmuir 2022, 38, 8805−8816

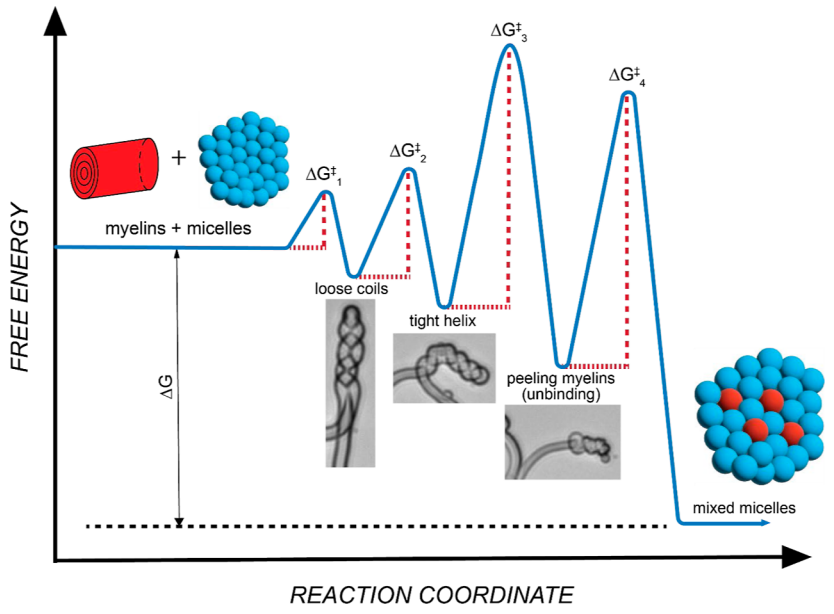

Figure 5. Free-energy landscape of detergent-mediated myelin solubilization. A cartoon representation of the kinetic pathway of detergent-mediated myelin solubilization. The pathway is dotted with a sequence of metastable intermediates consisting of loose coils, tight helices, and peeled myelins in the order of decreasing free energy and increasing activation energy barriers until reaching the final state of a micellar suspension characterizing the equilibrium (adapted from ref 71). ΔG represents the overall driving force, and individual $\Delta G^{\ddagger}$ are the local activation energy barriers.

these lipid mixtures are not compositionally identical to the bulk stoichiometry.[41] Instead, the molecules segregate differentially: the outermost lamellae are more enriched in cholesterol and sphingomyelin (L_o phase components), and the L_d phase forming POPC populates the innermost layers. This radial gradient in composition creates gradients in membrane fluidity and bending rigidities, with the outermost layers exhibiting the highest bending rigidity and the lowest lateral fluidity. In these structurally dense L_o phases, surfactants and detergents have weak solubility and may promote intralayer domain formation by segregating cholesterol and sphingomyelin from the detergent and any fluid-phase POPC lipids.[63−66] Based on these considerations, we propose that the reduced surfactant partitioning within the L_o phase lipids and the differential membrane bending properties might explain the observed suppression of the coiling instability in cholesterol-rich myelin layers.

Next, what dictates the thinning regime? Both single-component and multicomponent myelin figures exhibit a monotonic decrease in myelin widths. In the single-component myelins, this thinning regime usually follows the tightening regime, but we also observed overlaps between the two. This overlap manifests as the coil tightening at fixed pitch angles, which require the two processes—a decrease in pitch size (tightening) and a decrease in a tube's diameter (thinning)—to become fully congruent with one another. In the case of multicomponent myelins, where the coiling stage is suppressed, the thinning occurs continuously, often extending and overlapping with the next stage characterized by myelin retraction or detachment. In both experimental cases, the observed thinning requires delamination of lamellae from the cylindrical, smectic, multilamellar myelins, a process consistent with the previously studied phenomenon of complete unbinding transitions in which thermal fluctuations and local short-range interactions can drive unbinding of lamellae in smectic phases.[50,67,68] Although our experiments do not resolve the kinetic pathways by which thinning proceeds, the partitioning characteristics of DDAPS suggest a plausible route: the asymmetric accumulation of DDAPS in the outer leaflet of the exposed myelin bilayer (see above) and the increased flip-flop of lipids then sets the stage for lamella delamination via the so-called micellar mechanism.[22] Here, the lipids are extracted from the surfactant-doped outer leaflet of the exposed bilayer of myelins via interactions with the detergent micelles. The resulting depletion of lipids exposes the nonpolar interstitial space of a bilayer which prompts increased rates of lipid flip-flopping for energetic balance, driving further dissolution of the exposed bilayer. With each successive delamination, new bilayers become exposed to the detergent micelles, driving a stepwise cascade of myelin thinning, such as what was observed.

Last, why does the system choose to retract or detach? As a simultaneously elastic and fluid structure, myelin figures are dynamic and complicated. As deduced previously, myelin growth can be determined by its hydration potential; therefore, we elongate this rationality and propose that myelin retracts (or reversibly grows) depending on each individual tube's hydration properties.[32] Contrarily, the striking topological transition characterizing the detachment of multicomponent myelins and the appearance of free-floating myelins is a novel observation. For the myelinic protrusions to detach from the source lipid mass, an energy-intensive topological transition—a pinch-off event—in the vicinity of the myelinic root is needed. At present, we do not fully understand the mechanisms driving this localized fission. However, it is tempting to speculate that the roots of the myelins—which can be expected to be at lower steady-state tension in growing myelins (out of equilibrium) because of the frictional drag induced by the water flow—provide localized spatial and compositional niches for surfactant intercalation, creating conditions for rupture.[69,70] This proposition, however, is unverified.

https://doi.org/10.1021/acs.langmuir.2c00774
Langmuir 2022, 38, 8805−8816

With these complexities elucidated, how do they couple to form this solubilization pathway? *En route* to dissolution of single-component myelin, we observed the development of a well-defined sequence of kinetic intermediates: (1) loose coiled helices, upon surfactant intercalation and spontaneous curvature generation in the exposed bilayer; (2) maximally coiled tight helices, which increase membrane contact and adhesion; and (3) peeled myelins, reflecting stepwise delamination of external lamellae. Their appearance suggests a plausible pathway for the solubilization of myelin figures. We propose that the pathway to the solubilization of myelins is marked by multiple free-energy steps, each with its own activation energy barrier and each providing a corresponding lowering of the system's free energy (Figure 5).[71] First ($\Delta G_1^{\ddagger}$), DDAPS intercalates within the exposed bilayers of the myelin figures, reorganizing the lipid packing within the hydrophobic interior, producing local spontaneous curvature, and bending the bilayers of the myelin tube. These processes are antagonized by the interleaflet interactions, interlamellar Helfrich interactions, and elastic bending strain considerations of the tube, leading to the loose coiled step.[28,58] Next ($\Delta G_2^{\ddagger}$), the subsequent insertion of higher amounts of DDAPS more intensely bends the bilayers, further aggravating the factors mentioned for $\Delta G_1^{\ddagger}$ and increasing the activation energy of the step to access the tightened stage. In possible contrast, the increased contact line of tightened myelin helices presents the opportunity for a beneficial interaction energy between the surface bilayers.[54] Also, each intermediate is stabilized by their increasing magnitude of spontaneous curvature.[58,72] Upon reaching solubilizing circumstances ($\Delta G_3^{\ddagger}$), we anticipate the highest value of activation energy to reach the peeling step. In this step, mixed micelles begin leaving the mother mesophase and, as the mother lipid material is lost, the hydrophobic core becomes exposed to external aqueous conditions and the zwitterionic lipids flip-flop to relieve this thermodynamic consequence.[73] These interactions, as well as considerations in elastic bending strain and Helfrich interactions seen in the previous steps, maximize the activation energy.[58,72] In return, entropy will be maximized by the mixing of the participating amphiphiles between phases and the translational degrees of freedom gained when the mixed micelles are removed from the lamellar phase.[72] Lastly ($\Delta G_4^{\ddagger}$), we anticipate that the energetic procession of peeling myelins to an isotropic solution of mixed micelles will be smaller in value than $\Delta G_3^{\ddagger}$. While incurring the same processes, the quantitative magnitude of the participating interactions will decrease as less mother lipid material is left. Overall (ΔG), this process occurs due to the complex balance of spontaneous curvature, interlamellar Helfrich interactions, elastic bending strain, the hydrophobic effect, possible adhesive interactions, available thermal energy, and entropy maximization of the involved components.[72] Thus, it appears that the observed multistage process of myelin solubilization loosely parallels Ostwald's rule of stages and the Stranski–Totomanow conjecture, traditionally employed for the crystallization of molecules instead of the behavior of liquid-crystalline materials, where a phase transition occurs when its proceeds through the smallest loss of free energy to its immediate precursor by the smallest available activation energy barrier.[42,74]

CONCLUSIONS

The solubilization of the chemically homogeneous, single-component myelins (such as those obtained by the hydration of fluid-phase POPC lipids) by a common zwitterionic detergent (DDAPS) begins with the appearance of an axial twist, which propagates to produce transient, but long-lived, extended helices. Over time, these helices *tighten*, increasing membrane line contact; *become thin*, gradually shedding lamellae; and *retract*, remixing with the source lipid mass while solubilizing into the aqueous phase. In contrast, multicomponent myelin figures (composed of an equimolar mixture of POPC, SM, and CHOL) did not exhibit any observable helical morphogenesis, but thinned and *retracted* or *detached*, producing free-floating myelins. While distinct, these metastable steps were observed to occasionally happen concurrently; measuring the pitch angle of certain coiled myelin figures elicited the possibility of tubes having congruent tightening and thinning with an average angle of 39°. During this solubilization process, a multitude of factors dictated the kinetics, including the mass transfer of both pure DDAPS micelles to and mixed micelles from the parent mesophase, the partitioning of DDAPS molecules into bilayers from the aqueous phase, the intercalation properties of DDAPS within a bilayer, and the energetically intensive bending of bilayers within the myelin figure. The combination of these factors explains why solubilization rates appear to be independent of concentration.

These metastable states are segregated due to their thermodynamic considerations, including spontaneous curvature, the elastic bending of membrane bilayers, and the interlamellar Helfrich interactions. The partitioning and asymmetric accumulation of DDAPS in the outer leaflet of the exposed myelin bilayer induces a heterogeneous spontaneous curvature and desire for the populated bilayer to bend. The morphological change competes with the interlamellar Helfrich interactions holding the bilayers together, with tighter curvatures (or deviations from unperturbed bilayers), increasing the energetic cost. Upon reaching solubilizing concentrations within the bilayer, the system enacts the micellar mechanism where mixed micelles leave the bilayer organization and remove the parent lipid material, inducing an increased rate of flip-flopping lipids to minimize exposure to the external aqueous phase. As the parent lipid material is lost, lamellae can delaminate, solubilize, and expose the internal bilayers to the new pure DDAPS micelles. This occurs iteratively until the myelin figure has been fully destroyed or retracted. The solubilization of myelin by this proposed mechanism of energetic considerations possibly parallels the procedures of Ostwald's rule of stages.

While similarly exposed to pure DDAPS micelles, multicomponent myelins incur alternate mechanisms of morphological destruction. The helical morphogenesis is shunted in favor of thinning, and retraction or detachment. We propose that the reduced surfactant partitioning within the eternal L_o phase lipids and the differential membrane properties might explain the observed suppression of the coiling instability in cholesterol-rich myelin layers.

Our findings that the pathways of surfactant-mediated solubilization of multilamellar lipid mesophases are dotted with long-lived or metastable intermediates of well-defined morphologies—such as those that may be predicted by extending Ostwald's rule of stages—may open interesting new possibilities. They suggest new pathways for deriving novel classes of transiently organized and surfactant-programmable mesostructures and self-assemblies outside the thermal equilibrium.[75,76] They might prove valuable in extending the

https://doi.org/10.1021/acs.langmuir.2c00774
Langmuir 2022, 38, 8805−8816

tool kit for *in meso* crystallogenesis—a rapidly evolving field for crystallizing membrane proteins within lipid environments.[15,77,78]

MATERIALS AND METHODS

Materials. POPC, 1,2-dioleoyl-*sn*-glycero-3-phosphoethanolamine-*N*-(lissamine rhodamine B sulfonyl) (ammonium salt) (Rho B-DOPE), 1,2-dipalmitoyl-*sn*-glycero-3-phosphoethanolamine-*N*-(7-nitro-2-1,3-benzoxadiazol-4-yl) (ammonium salt) (NBD-DPPE), SM, and CHOL were purchased from Avanti Polar Lipids (Alabaster, AL). DDAPS was acquired from Millipore Sigma (Burlington, MA). Chloroform, methanol, ethanol (denatured), and sucrose were purchased from Sigma-Aldrich (St. Louis, MO). Base and cover borosilicate microscope slides were obtained from Corning (Corning, NY). Nitrogen gas was acquired from Praxair (Danbury, CT). Indium tin oxide (ITO)-coated glass slides (resistance 4−30 Ω) were purchased from Delta Technologies (Loveland, CO). Eight-well plastic-bottom plates were obtained from MatTek Corp. (Ashland, MA). All chemicals were used without further purification.

Myelin Preparation and Experimentation. Myelin figures were prepared by adopting a previously reported procedure of hydrating a dried mass of phospholipid molecules between two microscope slides.[32] Two separate stock solutions were prepared at a concentration of 25 mg/ml in 9:1 (v/v) chloroform to methanol, (1) 100% POPC and (2) an equimolar (1:1:1) ratio of POPC, SM, and CHOL with 0.3% NBD-DPPE and 0.1% Rho B-DOPE. Microscope slides were cleaned by sonication for 5 min in a bath of ethanol, dipping in chloroform for 1 s, and drying with nitrogen gas and desiccation. Small droplets (4 μL) of stock solution were placed on cleaned cover slides, and the solution was allowed to dry in the atmosphere until a dried mass remained (∼15 min). Droplets containing fluorescent labels were covered with aluminum foil to protect them from light while drying. Coated cover slides and clean base slides were then pressed together into a lipid cake for 10 s using a Mettler Toledo (Greifensee, Switzerland) presser. Cakes were either used immediately or stored under a house vacuum and protected from prolonged exposure to ambient light. All cakes were used within a week of preparation.

Lipid cakes were mounted onto the appropriate microscopy instrument, and a sharp, unobstructed edge of the dried mass was found (Figure S5). 40 μL of an aqueous solution was then pipetted onto the edge of the sandwich, and the solution moved into the gap by advection with the glass. Upon contact with the dried mass, tubules of myelin figures grew outwardly into the surrounding area. The lipid cake could be hydrated with deionized water, DDAPS at varying concentrations, or a two-step process of 40 μL of deionized water and then 40 μL of 120 mM DDAPS after 5 min. All experiments were carried out at room temperature, which is above the gel-fluid phase transition temperature of almost all of the lipids used. SM, possessing a transition temperature of 37 °C, posed no issues during myelin formation once assembled with aqueous solutions.[41]

To confirm the surface nature of the surfactant's interactions, myelin was assembled using the two-step process (see above). Five minutes was chosen for step 2 because tubes seldomly intake the external aqueous solution and grow at that time. Thus, the incoming DDAPS (in the micellar phase) is limited to interacting with the surface bilayers of the myelins. Within 5−10 min, myelins began to coil qualitatively comparable to the previous exposure methods (Figure S2).

GUV Preparation and Experimentation. GUVs were prepared in alignment with previously established techniques using electroformation.[79] Two separate stock solutions were prepared at a concentration of 2 mg/ml in chloroform, (1) 100% POPC and (2) an equimolar (1:1:1) ratio of POPC, SM, and CHOL with 3% NBD-DPPE and 1% Rho B-DOPE dopants. 15 μL of the desired stock solution was spread on the conductive side of two ITO-coated microscope slides and dried for at least 2 h under a house vacuum. Once dried, a rubber "O" ring (Ace Hardware, Davis, CA) was glued to one slide around the lipid film using vacuum grease (Dow Corning, Midland, MI) and about 1 mL of a 10 mM sucrose solution was added to the cavity. The chamber was then sealed with the other conductive slide to be water-tight with no air bubbles inside. With a function generator, a 4 Vpp AC sine-wave current was applied across both slides at 10 Hz for 1.5 h. Afterward, the current was switched to a 4 Vpp square-wave current at 2 Hz for 1.5 h. Throughout current application, slides were covered with aluminum foil to minimize light exposure. Slides with lipid films of stock solution (2) were heated to 45 °C on a hot plate, while slides with lipid films of stock solution (1) were kept at room temperature during current application. Once finished, the sealed system was disassembled, and the solution of vesicles was transferred to a separate vial. The giant vesicles were then stored at 4 °C for 2 days before use.

Eight-well plates were mounted on the appropriate microscopy instrument, and 200 μL of the desired DDAPS solution (1, 15, or 120 mM) was added to a well. Giant vesicles were added to the solution at the bottom of the sample chamber, and the resulting dynamics were visualized.

Brightfield Microscopy. Brightfield microscopy measurements were performed using a Nikon Eclipse TE2000S inverted fluorescence microscope (Technical Instruments, Burlingame, CA) equipped with a Roper Cool Snap charge-coupled device (CCD) camera (Technical Instruments). Videos were taken using a Plan Fluor 20X (NA, 0.25) objective (Nikon, Japan).

Spinning-Disk Confocal Fluorescence Microscopy. Spinning-disk confocal fluorescence microscopy measurements were performed using an Intelligent Imaging Innovations Marianas Digital Microscopy workstation (3i Denver, CO) fitted with a CSU-X1 spinning disk head (Yokogawa Musashino-sh, Tokyo, Japan) and a Quantem512SC EMCCD camera (Photometrics Tuscon, AZ). Fluorescence micrographs were obtained using a Zeiss Plan Fluor 63x (NA 1.4) oil immersion objective (Carl Zeiss Oberkochen, Germany).

Wide-Field Fluorescence Microscopy. Wide-field fluorescence microscopy images of myelin figures were acquired using a Carl Zeiss Axio Observer Z1, fitted with an EC Plan-Neofluar 63x/1.25 oil objective (Carl Zeiss, Oberkochen, Germany) and equipped with Zeiss set 10 (Ex: 450−490; Em: 515−565) and Zeiss set 31 (Ex: 550−570; Em: 590−650), and a HXP 210 C mercury metal halide lamp (Carl Zeiss, Oberkochen, Germany).

Wide-field fluorescence microscopy measurements of giant vesicles were performed using a Nikon Eclipse TE2000S inverted fluorescence microscope (Technical Instruments, Burlingame, CA) equipped with a Roper Cool Snap CCD camera (Technical Instruments) and Hg lamp as a light source. Videos were taken using a Plan Fluor 20X (NA, 0.25) air objective (Nikon, Japan) and filter cubes to filter the absorption and emission of the source and camera.

Analysis of Myelin. All images and videos were analyzed using the ImageJ software package. Helical morphogenesis, degradation rates, widths, diffusion coefficients, and handedness were computed by manual measurements or calculations.

ASSOCIATED CONTENT

Supporting Information

The Supporting Information is available free of charge at https://pubs.acs.org/doi/10.1021/acs.langmuir.2c00774.

Myelin front growth over time, proposed intermediates of surfactant-mediated myelin solubilization, definition and analysis of the pitch angle of myelin helices, lifetime of a myelin figure expressing proposed intermediates, and satisfactory "lipid cakes" (PDF)

Spontaneous coiling of a single-component myelin (AVI)

POPC GUV bursting during 1 mM DDAPS exposure (AVI)

POPC GUV bursting during 15 mM DDAPS exposure (AVI)

https://doi.org/10.1021/acs.langmuir.2c00774
Langmuir 2022, 38, 8805−8816

POPC GUV bursting during 120 mM DDAPS exposure (AVI)
POPC:SM:CHOL GUV bursting during 1 mM DDAPS exposure (AVI)
POPC:SM:CHOL GUV bursting during 15 mM DDAPS exposure (AVI)
Complicated morphologies of surfactant interactions with myelin figures (AVI)
Myelin length recruitment for coiling during 60 mM DDAPS exposure (AVI)
Myelin length recruitment for coiling during 90 mM DDAPS exposure (AVI)
Myelin figures utilizing the growth regime for coiling (AVI)
Helices of myelin figures tightening when exposed to 120 mM DDAPS (AVI)
Helices of myelin figures tightening when exposed to 90 mM DDAPS (AVI)
Helices of myelin figures tightening when exposed to 60 mM DDAPS (AVI)
Lifetime of a myelin figure expressing proposed intermediates (AVI)
Multicomponent myelin thinning and retraction (AVI)
Multicomponent myelin thinning (AVI)
Detachment of a myelin figure during solubilization when exposed to 90 mM DDAPS (AVI)
Multicomponent myelin figures with a 1:2:2 ratio of POPC, SM, and CHOL (AVI)
Multicomponent myelin figures with 3:1:1 M ratio of POPC, SM, and CHOL (AVI)

AUTHOR INFORMATION

Corresponding Author

Atul N. Parikh − *Chemistry Graduate Group and Department of Biomedical Engineering, University of California, Davis, Davis, California 95616, United States; Singapore Centre for Environmental Life Sciences Engineering, Nanyang Technological University, Singapore 637551, Singapore;* orcid.org/0000-0002-5927-4968; Email: anparikh@ucdavis.edu

Authors

Daniel J. Speer − *Chemistry Graduate Group, University of California, Davis, Davis, California 95616, United States*

James C. S. Ho − *Singapore Centre for Environmental Life Sciences Engineering, Nanyang Technological University, Singapore 637551, Singapore*

Complete contact information is available at: https://pubs.acs.org/10.1021/acs.langmuir.2c00774

Author Contributions

D.J.S. and A.N.P. designed research; D.J.S. and J.C.S.H. performed microscopy experiments; D.J.S. analyzed data; D.J.S., J.C.S.H., and A.N.P. wrote the manuscript.

Funding

This work is supported by a grant from the National Science Foundation (DMR-2104123). The contributions of JH are supported by the Singapore Centre for Life Science Engineering (SCELSE).

Notes

The authors declare no competing financial interest.

ACKNOWLEDGMENTS

We would like to thank Pallavi Sambre and Dr. Padmini Rangamani for their productive conversations. The 3i Marianas spinning-disk confocal fluorescence instrument used in this study was purchased using NIH Shared Instrumentation grant 1S10RR024543-01. We thank the MCB Light Microscopy Imaging Facility, which is a UC Davis Campus Core Research Facility, for the use of this microscope.

ABBREVIATIONS

DDAPS, *n*-dodecyl-*N*,*N*-dimethyl-3-ammonio-1-propanesulfonate; POPC, 1-palmitoyl-2-oleoyl-*sn*-glycero-3-phosphocholine; Rho B-DOPE, 1,2-dioleoyl-*sn*-glycero-3-phosphoethanolamine-*N*-(lissamine rhodamine B sulfonyl) (ammonium salt); NBD-DPPE, 1,2-dipalmitoyl-*sn*-glycero-3-phosphoethanolamine-*N*-(7-nitro-2-1,3-benzoxadiazol-4-yl) (ammonium salt); SM, egg sphingomyelin; CHOL, cholesterol; CMC, critical micelle concentration; L_o, liquid-ordered phase; L_d, liquid-disordered phase

REFERENCES

(1) Israelachvili, J. N.; Mitchell, D. J.; Ninham, B. W. Theory of self-assembly of hydrocarbon amphiphiles into micelles and bilayers. *J. Chem. Soc., Faraday Trans. 2* **1976**, *72*, 1525−1568.
(2) Israelachvil, J. N. *Intermolecular and Surface Forces*, 3rd ed.; Academic Press: Cambridge, MA, 2011.
(3) Ben-Shaul, A.; Gelbart, W. M. Theory of chain packing in amphiphilic aggregates. *Annu. Rev. Phys. Chem.* **1985**, *36*, 179−211.
(4) Nagarajan, R.; Ruckenstein, E. Theory of surfactant self-assembly: a predictive molecular thermodynamic approach. *Langmuir* **1991**, *7*, 2934−2969.
(5) Chandler, D. Interfaces and the driving force of hydrophobic assembly. *Nature* **2005**, *437*, 640−647.
(6) Heerklotz, H. Interactions of surfactants with lipid membranes. *Q. Rev. Biophys.* **2008**, *41*, 205−264.
(7) Lichtenberg, D. Characterization of the solubilization of lipid bilayers by surfactants. *Biochim. Biophys. Acta* **1985**, *821*, 470−478.
(8) Helenius, A.; Simons, K. Solubilization of Membranes by Detergents. *Biochim. Biophys. Acta* **1975**, *415*, 29−79.
(9) Nomura, F.; et al. Capabilities of liposomes for topological transformation. *Proc. Natl. Acad. Sci. U.S.A.* **2001**, *98*, 2340−2345.
(10) Ngassam, V. N.; Howland, M. C.; Sapuri-Butti, A.; Rosidi, N.; Parikh, A. N. A comparison of detergent action on supported lipid monolayers and bilayers. *Soft Matter* **2012**, *8*, 3734−3738.
(11) Urbaneja, M. A.; et al. Detergent solubilization of phospholipid vesicle. Effect of electric charge. *Biochem. J.* **1990**, *270*, 305−308.
(12) Lichtenberg, D.; Robson, R. J.; Dennis, E. A. Solubilization of phospholipids by detergents structural and kinetic aspects. *Biochim. Biophys. Acta* **1983**, *737*, 285−304.
(13) Chabanon, M.; Rangamani, P. Solubilization kinetics determines the pulsatory dynamics of lipid vesicles exposed to surfactant. *Biochim. Biophys. Acta, Biomembr.* **2018**, *1860*, 2032−2041.
(14) Bordier, C. Phase separation of integral membrane proteins in Triton X-114 solution. *J. Biol. Chem.* **1981**, *256*, 1604−1607.
(15) Seddon, A. M.; Curnow, P.; Booth, P. J. Membrane proteins, lipids and detergents: not just a soap opera. *Biochim. Biophys. Acta, Biomembr.* **2004**, *1666*, 105−117.
(16) Garavito, R. M.; Ferguson-Miller, S. Detergents as tools in membrane biochemistry. *J. Biol. Chem.* **2001**, *276*, 32403−32406.
(17) Silvius, J. R. Solubilization and functional reconstitution of biomembrane components. *Annu. Rev. Biophys. Biomol. Struct.* **1992**, *21*, 323−348.
(18) London, E.; Brown, D. A. Insolubility of lipids in Triton X-100: physical origin and relationship to sphingolipid/cholesterol membrane domains (rafts). *Biochim. Biophys. Acta* **2000**, *1508*, 182−195.

(19) Brown, D. A.; London, E. Structure and function of sphingolipid- and cholesterol-rich membrane rafts. *J. Biol. Chem.* **2000**, *275*, 17221−17224.
(20) Ahmed, S. N.; Brown, D. A.; London, E. On the Origin of Sphingolipid/Cholesterol-Rich Detergent-Insoluble Cell Membranes: Physiological Concentrations of Cholesterol and Sphingolipid Induce Formation of a Detergent-Insoluble, Liquid-Ordered Lipid Phase in Model Membranes. *Biochemistry* **1997**, *36*, 10944−10953.
(21) Lichtenberg, D.; Ahyayauch, H.; Goñi, F. M. The mechanism of detergent solubilization of lipid bilayers. *Biophys. J.* **2013**, *105*, 289−299.
(22) Kragh-Hansen, U.; le Maire, M.; Møller, J. V. The mechanism of detergent solubilization of liposomes and protein-containing membranes. *Biophys. J.* **1998**, *75*, 2932−2946.
(23) Hamada, T.; et al. Physicochemical Profiling of Surfactant-Induced Membrane Dynamics in a Cell-Sized Liposome. *J. Phys. Chem. Lett.* **2012**, *3*, 430−435.
(24) Heerklotz, H.; Binder, H.; Lantzsch, G.; Klose, G.; Blume, A. Lipid/Detergent Interaction Thermodynamics as a Function of Molecular Shape. *J. Phys. Chem. B* **1997**, *101*, 639−645.
(25) Nazari, M.; Kurdi, M.; Heerklotz, H. Classifying surfactants with respect to their effect on lipid membrane order. *Biophys. J.* **2012**, *102*, 498−506.
(26) Toyota, T.; et al. Fluorescence Microscopic Investigation on Morphological Changes of Giant Multilamellar Vesicles Induced by Amphiphilic Additives. *Langmuir* **2006**, *22*, 1976−1981.
(27) Sudbrack, T. P.; Archilha, N. L.; Itri, R.; Riske, K. A. Observing the Solubilization of Lipid Bilayers by Detergents with Optical Microscopy of GUVs. *J. Phys. Chem. B* **2011**, *115*, 269−277.
(28) Lis, L. J.; McAlister, M.; Fuller, N.; Rand, R. P.; Parsegian, V. A. Interactions Between Neutral Phospholipid Bilayer Membranes. *Biophys. J.* **1982**, *37*, 657−665.
(29) Sakurai, I.; Kawamura, Y.; Sakurai, T.; Ikegami, A.; Seto, T. Morphology and Growth Behaviour of Myelin Figures of Lecithin. *Mol. Cryst. Liq. Cryst.* **1985**, *130*, 203−222.
(30) Sakurai, I.; Suzuki, T.; Sakurai, S. Cross-sectional view of myelin figures. *Biochim. Biophys. Acta* **1989**, *985*, 101−105.
(31) Buchanan, M.; Egelhaaf, S. U.; Cates, M. E. Dynamics of Interface Instabilities in Nonionic Lamellar Phases. *Langmuir* **2000**, *16*, 3718−3726.
(32) Zou, L.-N. Myelin figures: the buckling and flow of wet soap. *Phys. Rev. E: Stat., Nonlinear, Soft Matter Phys.* **2009**, *79*, 061502.
(33) Benkowska-Biernacka, D.; Smalyukh, I. I.; Matczyszyn, K. Morphology of Lyotropic Myelin Figures Stained with a Fluorescent Dye. *J. Phys. Chem. B* **2020**, *124*, 11974−11979.
(34) Kennedy, A. P.; Sutcliffe, J.; Cheng, J.-X. Molecular composition and orientation in myelin figures characterized by coherent anti-stokes Raman scattering microscopy. *Langmuir* **2005**, *21*, 6478−6486.
(35) Stoeckenius, W. An electron microscope study of myelin figures. *J. Biophys. Biochem. Cytol.* **1959**, *5*, 491−500.
(36) Tsafrir, I.; Guedeau-Boudeville, M.-A.; Kandel, D.; Stavans, J. Coiling instability of multilamellar membrane tubes with anchored polymers. *Phys. Rev. E: Stat., Nonlinear, Soft Matter Phys.* **2001**, *63*, 031603.
(37) Lee, Y.-C.; et al. Impact of Detergents on Membrane Protein Complex Isolation. *J. Proteome Res.* **2018**, *17*, 348−358.
(38) Kum, S. L.; Ho, J. C. S.; Parikh, A. N.; Liedberg, B. Amphiphilic Membrane Environments Regulate Enzymatic Behaviors of Salmonella Outer Membrane Protease. *ACS Bio Med Chem Au* **2022**, *2*, 73.
(39) Nollstadt, K. H.; et al. Potential of the sulfobetaine detergent zwittergent 3-12 as a desorbing agent in biospecific and bioselective affinity chromatography. *J. Chromatogr.* **1989**, *497*, 87−100.
(40) Church, W. R.; Ebner, K. E. Solubilization of prolactin receptor by a Zwitterionic detergent. *Experientia* **1982**, *38*, 434−435.
(41) Ho, J. C. S.; Su, W.-C.; Chun Wang, X.; Parikh, A. N.; Liedberg, B. Nonequilibrium Self-Organization of Lipids into Hierarchically Ordered and Compositionally Graded Cylindrical Smectics. *Langmuir* **2022**, *38*, 1045−1056.
(42) Ostwald, W. Studien über die Bildung und Umwandlung fester Körper. *Z. Phys. Chem.* **1897**, *22U*, 289−330.
(43) Sakurai, I.; Kawamura, Y. Growth mechanism of myelin figures of phosphatidylcholine. *Biochim. Biophys. Acta* **1984**, *777*, 347−351.
(44) Reissig, L.; et al. Three-dimensional structure and growth of myelins. *Langmuir* **2010**, *26*, 15192−15199.
(45) Sakurai, I.; Suzuki, T.; Sakurait, S. Structure and Growth Behavior of Myelin Figures. *Mol. Cryst. Liq. Cryst.* **1990**, *180*, 305−311.
(46) Mishima, K.; Yoshiyama, K. Growth rate of myelin figures of egg-yolk phosphatidylcholine. *Biochim. Biophys. Acta* **1987**, *904*, 149−153.
(47) Mishima, K.; Ogihara, T.; Tomita, M.; Satoh, K. Growth rate of myelin figures for phosphatidylcholine and phosphatidylethanolamine. *Chem. Phys. Lipids* **1992**, *62*, 87−91.
(48) Dave, H.; Surve, M.; Manohar, C.; Bellare, J. Myelin growth and initial dynamics. *J. Colloid Interface Sci.* **2003**, *264*, 76−81.
(49) Lin, K.-C.; Weis, R. M.; McConnell, H. M. Induction of helical liposomes by ca2+-mediated intermembrane binding. *Nature* **1982**, *296*, 164−165.
(50) Lipowsky, R.; Leibler, S. Unbinding transitions of interacting membranes. *Phys. Rev. Lett.* **1986**, *56*, 2541−2544.
(51) Petrache, H. I.; Dodd, S. W.; Brown, M. F. Area per Lipid and Acyl Length Distributions in Fluid Phosphatidylcholines Determined by 2H NMR Spectroscopy. *Biophys. J.* **2000**, *79*, 3172−3192.
(52) Schuck, S.; Honsho, M.; Ekroos, K.; Shevchenko, A.; Simons, K. Resistance of cell membranes to different detergents. *Proc. Natl. Acad. Sci. U.S.A.* **2003**, *100*, 5795−5800.
(53) Lichtenberg, D.; Goñi, F. M.; Heerklotz, H. Detergent-resistant membranes should not be identified with membrane rafts. *Trends Biochem. Sci.* **2005**, *30*, 430−436.
(54) Mishima, K.; Fukuda, K.; Suzuki, K. Double helix formation of phosphatidylcholine myelin figures. *Biochim. Biophys. Acta* **1992**, *1108*, 115−118.
(55) Sakurai, I.; Kawamura, Y.; Sakurai, T.; Ikegami, A.; Seto, T. Morphology and Growth Behaviour of Myelin Figures of Lecithin. *Mol. Cryst. Liq. Cryst.* **1985**, *130*, 203−222.
(56) Frette, V.; et al. Coiling of cylindrical membrane stacks with anchored polymers. *Phys. Rev. Lett.* **1999**, *83*, 2465−2468.
(57) Santangelo, C. D.; Pincus, P. Coiling instabilities of multilamellar tubes. *Phys. Rev. E: Stat., Nonlinear, Soft Matter Phys.* **2002**, *66*, 061501.
(58) Helfrich, W. Elastic Properties of Lipid Bilayers: Theory and Possible Experiments. *Z. Naturforsch. C* **1973**, *28*, 693−703.
(59) Hurault, J. P. Static distortions of a cholesteric planar structure induced by magnetic or ac electric fields. *J. Chem. Phys.* **1973**, *59*, 2068−2075.
(60) Pantaler, E.; Kamp, D.; Haest, C. W. M. Acceleration of phospholipid flip-flop in the erythrocyte membrane by detergents differing in polar head group and alkyl chain length. *Biochim. Biophys. Acta, Biomembr.* **2000**, *1509*, 397−408.
(61) Sheetz, M. P.; Singer, S. J. Biological Membranes as Bilayer Couples. A Molecular Mechanism of Drug-Erythrocyte Interactions. *Proc. Natl. Acad. Sci. U.S.A.* **1974**, *71*, 4457−4461.
(62) Needham, D.; Zhelev, D. V. Lysolipid Exchange with Lipid Vesicle Membranes. *Ann. Biomed. Eng.* **1995**, *23*, 287−298.
(63) Heerklotz, H.; Szadkowska, H.; Anderson, T.; Seelig, J. The sensitivity of lipid domains to small perturbations demonstrated by the effect of triton. *J. Mol. Biol.* **2003**, *329*, 793−799.
(64) Wang, J.; Megha; London, E. Relationship between sterol/steroid structure and participation in ordered lipid domains (lipid rafts): Implications for lipid raft structure and function. *Biochemistry* **2004**, *43*, 1010−1018.
(65) Schnitzer, E.; Kozlov, M. M.; Lichtenberg, D. The effect of cholesterol on the solubilization of phosphatidylcholine bilayers by the non-ionic surfactant Triton X-100. *Chem. Phys. Lipids* **2005**, *135*, 69−82.

https://doi.org/10.1021/acs.langmuir.2c00774
Langmuir 2022, 38, 8805−8816

(66) Mattei, B.; França, A. D. C.; Riske, K. A. Solubilization of Binary Lipid Mixtures by the Detergent Triton X-100: The Role of Cholesterol. *Langmuir* **2015**, *31*, 378−386.
(67) Netz, R. R. Complete unbinding of fluid membranes in the presence of short-ranged forces. *Phys. Rev. E* **1995**, *51*, 2286−2294.
(68) Leibler, S.; Lipowsky, R. Complete unbinding and quasi-long-range order in lamellar phases. *Phys. Rev. B* **1987**, *35*, 7004−7009.
(69) Pontes, B.; Monzo, P.; Gauthier, N. C. Membrane tension: A challenging but universal physical parameter in cell biology. *Semin. Cell Dev. Biol.* **2017**, *71*, 30−41.
(70) Nissen, J.; Gritsch, S.; Wiegand, G.; Rädler, J. O. Wetting of phospholipid membranes on hydrophilic surfaces - Concepts towards self-healing membranes. *Eur. Phys. J. B* **1999**, *10*, 335−344.
(71) Chung, S.-Y.; Kim, Y.-M.; Kim, J.-G.; Kim, Y.-J. Multiphase transformation and Ostwald's rule of stages during crystallization of a metal phosphate. *Nat. Phys.* **2009**, *5*, 68−73.
(72) Tanford, C. *The Hydrophobic Effect: Formation of Micelles and Biological Membranes*, 2nd ed.; Wiley: Hoboken, NJ, 1980.
(73) Andelman, D.; Kozlov, M. M.; Helfrich, W. Phase Transitions between Vesicles and Micelles Driven by Competing Curvatures. *Europhys. Lett.* **1994**, *25*, 231−236.
(74) Stranski, I. N.; Totomanow, D. Keimbildungsgeschwindigkeit und OSTWALDsche Stufenregel. *Z. Phys. Chem.* **1933**, *163A*, 399−408.
(75) Mattia, E.; Otto, S. Supramolecular systems chemistry. *Nat. Nanotechnol.* **2015**, *10*, 111−119.
(76) Mann, S. Self-assembly and transformation of hybrid nano-objects and nanostructures under equilibrium and non-equilibrium conditions. *Nat. Mater.* **2009**, *8*, 781−792.
(77) Cherezov, V.; Clogston, J.; Papiz, M. Z.; Caffrey, M. Room to move: Crystallizing membrane proteins in swollen lipidic mesophases. *J. Mol. Biol.* **2006**, *357*, 1605−1618.
(78) Landau, E. M.; Rosenbusch, J. P. Lipidic cubic phases: A novel concept for the crystallization of membrane proteins. *Proc. Natl. Acad. Sci. U.S.A.* **1996**, *93*, 14532−14535.
(79) Su, W.-C.; Gettel, D. L.; Chabanon, M.; Rangamani, P.; Parikh, A. N. Pulsatile Gating of Giant Vesicles Containing Macromolecular Crowding Agents Induced by Colligative Nonideality. *J. Am. Chem. Soc.* **2018**, *140*, 691−699.

https://doi.org/10.1021/acs.langmuir.2c00774
Langmuir 2022, 38, 8805−8816